Effects of substrate and ambient gas on epitaxial growth indium oxide thin films

M Nistor, W Seiler, C Hebert, E. Matei, Jacques Perrière

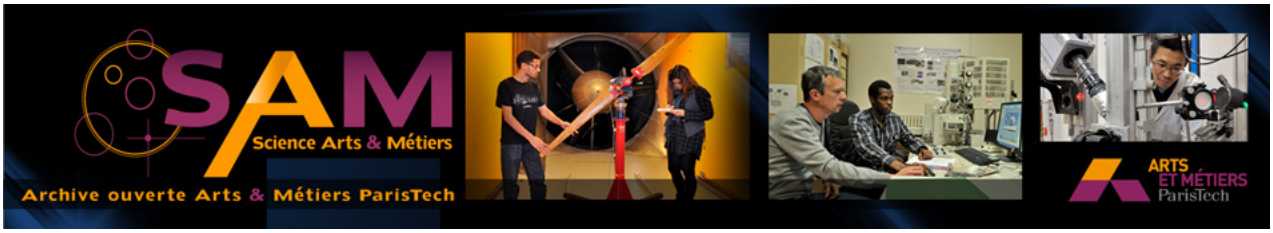

Effects of substrate and ambient gas on epitaxial growth indium oxide thin films

M. Nistor[a], W. Seiler[b], C. Hebert[c,d], E. Matei[e], J. Perrière[c,d,*]

[a] National Institute for Lasers, Plasma and Radiation Physics (NILPRP), Atomistilor Str. 109, L22 P.O. Box. MG-36, 077125 Bucharest-Magurele, Romania
[b] PIMM, UMR CNRS 8006 Arts et Métiers ParisTech, 151 Boulevard de l'Hopital, 75013 Paris, France
[c] Sorbonne Universités, UPMC Univ Paris 06, UMR 7588, INSP, F-75005 Paris, France
[d] CNRS, UMR 7588, INSP, F-75005 Paris, France
[e] National Institute of Materials Physics (NIMP), Atomistilor Str. 105 bis, P.O. Box MG-7, 077125 Magurele-Ilfov, Romania

A B S T R A C T

Indium oxide thin films were grown by pulsed electron beam deposition method at 500 °C on c-cut sapphire and (0 0 1) oriented $LaAlO_3$ single crystal substrates in oxygen or argon gas. The effects of ambient gas and substrate symmetry on the growth of indium oxide thin films were studied. Stoichiometric In_2O_3 films are formed in oxygen, while oxygen deficient $In_2O_{2.5}$ films are grown in argon, with In metallic nanoclusters embedded in a In_2O_3 matrix (nanocomposite films). In both cases, epitaxial In_2O_3 films having the bixbyite phase were grown with various orientation relationships, depending upon the substrate symmetry and gas ambient (oxygen or argon). Domain matching epitaxy was used to describe the precise in-plane epitaxial film–substrate relationships. The differences in film texture were correlated to the differences in growth conditions, while the differences in the film properties were correlated to the film oxygen composition.

Keywords:
Indium oxide
Thin films
Epitaxial growth
Nanocomposites
Pulsed electron beam deposition (PED)

1. Introduction

Owing to its specific optical (high transparency in the visible domain) and electrical (high conductivity) properties, indium oxide (In_2O_3) is used in a lot of applications in thin film form [1–4]. However, transport properties of this oxide are still a matter of discussion [5–8], and therefore the growth of In_2O_3 epitaxial thin films has been studied to determine their intrinsic physical properties [9–11]. The ideal substrate for the epitaxial growth of In_2O_3 thin films is cubic Y-stabilized ZrO_2 (YSZ) due to the small mismatch (1.7%) between the In_2O_3 bixbyite and the YSZ fluorite [11]. Such epitaxial In_2O_3 films on YSZ present interesting transport properties [12,13] with electron mobility as high as 226 $cm^2/V\,s$ [12]. Epitaxial In_2O_3 thin films were also obtained on c-cut sapphire substrate [10] despite the higher film–substrate mismatch, but the electron mobility was lower than that for the films grown on YSZ [9]. All these results were obtained on (1 1 1) oriented In_2O_3 films. From both applied and fundamental aspects, it is important to understand the pertinent factors affecting the structural characteristics and physical properties in epitaxial In_2O_3 films.

In this paper, we report thus on the study of the growth of In oxide films formed on different substrates and under different gas ambient (oxygen and argon). Two single crystal substrates were used: c-cut sapphire and (0 0 1) oriented cubic $LaAlO_3$. For the latter substrate, epitaxial indium oxide thin films were not reported yet. According to the differences in substrates symmetry, different film textures and microstructures are expected. Moreover, as the precise oxygen composition influences the nature, structure and properties of oxide films [14–16], the effect of oxygen deficiency in indium oxide films was also checked in this work. Pulsed electron beam deposition (PED) was used to grow such films since it allows the control of the oxygen incorporation in the films [15]. Epitaxial indium oxide films were thus obtained with texture and epitaxial relationships depending upon the substrate symmetry and growth conditions. These structural differences are related to the differences in the indium and oxygen fluxes reaching the surface of the growing film, while physical properties are mainly depending on the oxygen composition of the films.

2. Experimental

The In oxide films were grown on c-cut sapphire, (1 0 0) Si and (0 0 1) $LaAlO_3$ oriented substrates by the PED method in the experimental setup previously described [8–15]. The growth system

* Corresponding author at: Sorbonne Universités, UPMC Univ Paris 06, UMR 7588, INSP, F-75005 Paris, France. Tel.: +33 1 44 27 61 29; fax: +33 1 44 27 39 82.
E-mail address: jacques.perriere@insp.jussieu.fr (J. Perrière).

consists of a pulsed-electron beam source in the channel configuration delivering pulses with 100 ns duration and 2.5 J/cm^2 fluence. Films in the 50–700 nm thickness range were grown at 500 °C. The pulsed-electron beam ablated a high purity In_2O_3 target in pure Ar or O_2 gas at a 2×10^{-2} mbar pressure. After deposition, the films were cooled down at the gas pressure used for the growth.

The thickness and composition of the films were determined by Rutherford backscattering spectrometry (RBS), using the 2.5 MeV Van de Graaff accelerator of the SAFIR IBA Laboratory, University Pierre and Marie Curie. The precise film composition was obtained via the RUMP simulation program [17]. The surface morphology of the films was studied with a Zeiss EVO 50 scanning electron microscope (SEM). The crystalline structure of the films was studied by X-ray diffraction analyses (XRD) using the Philips Xpert diffractometer PIMM—Arts et Metiers ParisTech in Paris. The nature of the crystalline phases was studied by diffraction in the Bragg–Brentano geometry, and by asymmetric diffraction, i.e. pole figure measurements. In this last geometry, the epitaxial relationships between indium oxide films and single crystal substrates were studied and the precise in-plane orientations between film and substrate were determined. The optical transmittance of the films was measured in the UV–visible range by using a Cary 100 spectrophotometer. The nature, resistivity, concentration and mobility of the carriers were determined at room temperature with a MMR technologies Inc. Hall setup in the Van der Paw geometry at 3300 Gauss magnetic field.

3. Results

It has been previously reported that in pulsed-energy beam deposition methods like PED, the stoichiometry of the oxide films is controlled by the partial oxygen pressure during the growth [15,18,19]. Indeed, the flux of oxygen atoms reaching the surface of the growing film depends upon the oxygen partial pressure (PO_2), and as a result the incorporation of oxygen atoms is reduced when PO_2 is decreased. In this work, In oxide films have been grown under either Ar at a pressure (2×10^{-2} mbar) corresponding to a low PO_2 ($<10^{-5}$ mbar), or oxygen at 2×10^{-2} mbar. Hence, the oxygen concentration changed from the ideal In_2O_3 stoichiometry to a large oxygen deficiency $In_2O_{2.5}$, by solely changing the PO_2.

The growth in oxygen leads to dense, smooth and stoichiometric In_2O_3 films as determined by RBS analysis. However, owing to the accuracy of this method for light elements determination (4%), we cannot exclude a small oxygen deficiency in the films which can play a role on their physical properties [20]. A different behaviour was observed for the films grown at 500 °C in argon. Indeed, Fig. 1a represents the recorded RBS spectrum for such a film (square symbols), whose simulation via the RUMP program leads to an overall $In_2O_{2.5}$ composition (continuous line). This overall $In_2O_{2.5}$ composition does not mean that a specific chemical phase is present in the film. In fact, in RBS measurements, the absolute numbers of In and O atoms are determined independently of the nature of chemical phases. This means that $In_2O_{2.5}$ represents an average film composition. Moreover, the RBS spectrum shows that the film presents a rough surface morphology (as deduced from the width of the back edge of In spectrum and leading edge of the silicon substrate), and this conclusion was checked by the SEM analysis (Fig. 1c), which showed the presence of nanostructures (particles) with a size in the 50 to about few hundred nm range, giving a rough surface morphology. For comparison, the RBS spectrum recorded on a film grown at room temperature in argon pressure and its simulation are also presented in Fig. 1a, showing an abrupt back edge of In spectrum and leading edge of the Si substrate which corresponds to a smooth surface morphology, confirmed by the SEM image shown in Fig. 1(b). It can thus be concluded that particles present at the film surface are

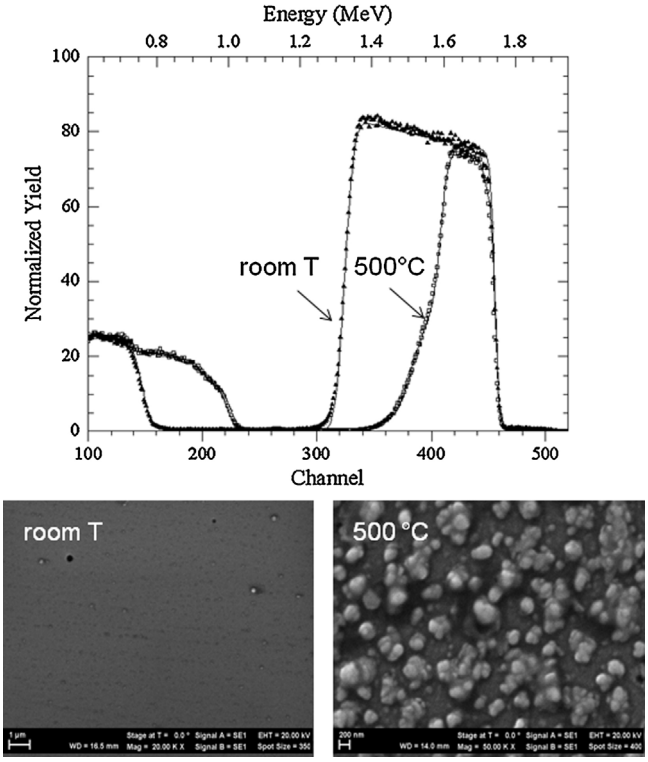

Fig. 1. (a) RBS spectra recorded (square symbols) for In_2O_3 films grown on Si substrates in argon at 500 °C and room temperature, respectively. The solid line corresponds to the simulated spectra; (b) SEM image of the surface morphology of a In_2O_3 film grown at room temperature and (c) SEM image of the surface morphology of a In_2O_3 film grown on Si substrate under argon at 500 °C substrate temperature.

thus certainly related to phenomena taking place at the film surface during the growth at elevated temperature. The driving force for the synthesis of these particles seems to be the temperature as the density and size of the particles were found to be increasing with the temperature. This could be due to the crystallization phenomenon associated with the increase in temperature. However, the temperature is not the sole parameter governing the nanostructure formation. Indeed, during PED film growth in oxygen at 500 °C (i.e. stoichiometric oxide film formation), such nanostructures are not present at the surface of the films. This indicates that the respective fluxes of indium and oxygen species reaching the film surface play a role on the surface nanostructures formation. The interpretation of this fact will be presented in the discussion part of the paper taking into account the X-ray diffraction results.

Under normal conditions, the In_2O_3 stable phase is the cubic bixbyite phase with 1.0118 nm lattice parameter. In_2O_3 is also known with the rhombohedral metastable phase (a = 5.478 Å and c = 14.51 Å), whose growth conditions have been recently studied [24]. In this work, we only observed the formation of the bixbyite In_2O_3 on c-cut sapphire or $LaAlO_3$ single crystal substrates, whatever being the gas during the PED growth.

Figs. 2 and 3 represent the XRD patterns registered on films grown in oxygen and argon on sapphire c-cut (Fig. 2) and $LaAlO_3$ (Fig. 3), respectively. The precise texture of the bixbyite phase depends upon the ambient gas during the growth and substrate. Indeed, in oxygen a (1 1 1) preferential growth is observed on c-cut sapphire (Fig. 2), while the (0 4 4) reflection peak with minor contribution from the (2 2 2) and (0 0 4) planes is observed on $LaAlO_3$ (Fig. 3). The growth in argon leads to the presence of the (2 2 2) and (0 0 4) peaks with similar intensities for the film grown on c-cut sapphire (Fig. 2). The comparison of the intensity ratio of the (0 0 4) and (2 2 2) peaks with the theoretical ratio given by the JCPDS file no. 1312-43-2, leads to the conclusion that about 75% of

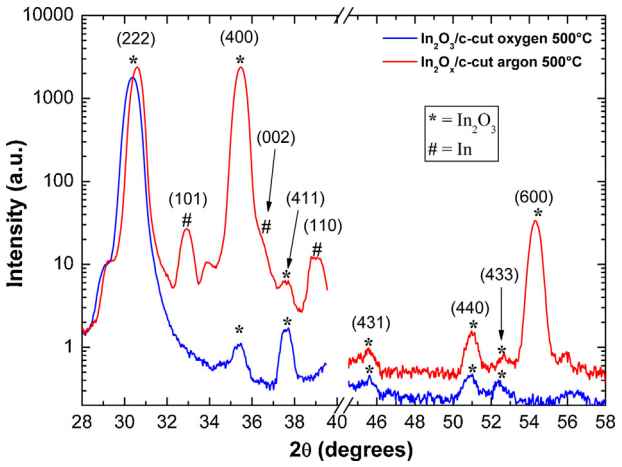

Fig. 2. X-ray diffraction patterns recorded for In_2O_3 films grown on c-cut sapphire substrates at 500 °C in O_2 and Ar.

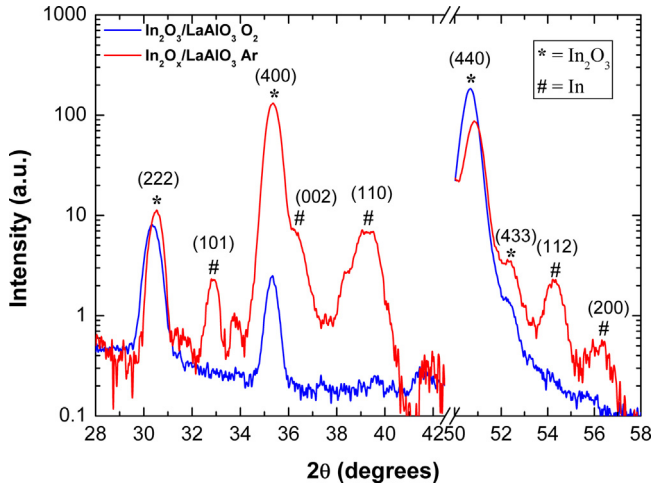

Fig. 3. X-ray diffraction patterns recorded for In_2O_3 films grown on $LaAlO_3$ substrates at 500 °C in O_2 and Ar.

the In_2O_3 crystallites in the film are (0 0 1) oriented. For the film grown under argon on $LaAlO_3$, the two main peaks correspond the (0 0 4) and (0 4 4) planes of the bixbyite In_2O_3, the (2 2 2) contribution being limited. From the intensity ratio of the (0 0 4) and (0 4 4) peaks, we can deduce that about 65% of the In_2O_3 crystallites on $LaAlO_3$ are (0 0 1) oriented. The axis parameter deduced from these patterns show that whatever the substrates, the films formed under argon present a parameter (1.0135 nm) close to the bulk value (1.0118 nm), while the growth under oxygen leads to a noticeable difference (1.0177 nm).

For the films grown under argon (Figs. 2 and 3), a peak is observed at approximately 33°, while it is not present in the XRD patterns for growth in oxygen. This peak could correspond to the (3 2 1) plane of the bixbyite phase ($2\theta = 33.103°$). However, it could also correspond to the (1 0 1) lattice reflection of the tetragonal metallic In phase ($2\theta = 32.964°$). Such a peak has been already observed in the case of largely oxygen deficient indium tin oxide films, and TEM experiments have confirmed the presence of In clusters in such films [22]. It appears thus reasonable to assume that the peak located at 33° corresponds to In clusters in the oxygen deficient $In_2O_{2.5}$ films. Moreover, other peaks are also identified with reflection planes of the tetragonal In phase in the X-ray pattern of the film grown on $LaAlO_3$ substrate, as observed in Figs. 2 and 3.

The formation of such clusters by phase separation was previously investigated in oxygen deficient oxide films [21,22,25–27].

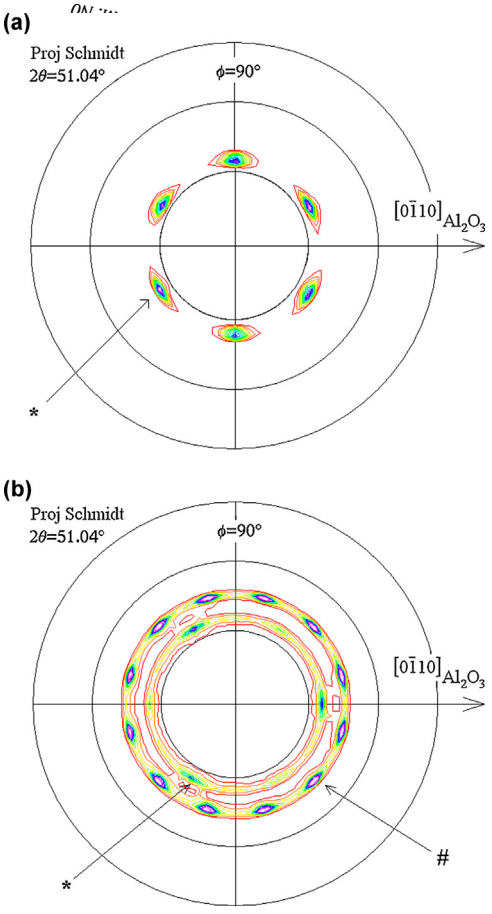

Fig. 4. Pole figures of the (0 4 4) In_2O_3 planes for films grown on c-cut sapphire substrates at 500 °C in O_2 (a) and Ar (b). In figure (a) and (b) the symbol * is assigned to six well defined poles at every 35.3° from the (0 4 4) reflection of the In_2O_3 crystallites (1 1 1) oriented. In figure (b) the symbol # is assigned to twelve well defined poles at every 45° from the (0 4 4) reflection of the In_2O_3 crystallites with the (0 0 1) texture.

Indeed, indium sub-oxides being not thermodynamically stable, oxygen deficient oxide films evolve towards the more stable phases, i.e. crystalline stoichiometric In_2O_3 and In metal. In this phase separation, the stable stoichiometric In_2O_3 phase grows at the expense of the sub-oxide, which becomes more and more oxygen deficient. In the extreme case of maximum oxygen deficiency, the phase separation leads to the formation of metallic clusters [15,21,22]. This phase separation can be written as following:

$$In_2O_{3-x} \rightarrow \left(1 - \frac{x}{3}\right) In_2O_3 + \left(\frac{2}{3}x\right) In, \quad (1)$$

leading to the formation of nanocomposite films with metallic clusters embedded in a stoichiometric matrix. This phenomenon explains the fact that the axis parameters of the In_2O_3 crystallites of the films grown in argon are close to the bulk value of the bixbyite phase due to stoichiometric In_2O_3 crystallites formation by the phase separation. In contrast, the films grown in oxygen contain oxygen vacancies which could be at the origin of the change in the axis parameter with respect to the bulk value.

The epitaxy of the films was studied, and Figs. 4 and 5 represent the pole figures of the (0 4 4) In_2O_3 planes ($2\theta = 51.04°$) for films grown on c-cut sapphire under oxygen (Fig. 4a) and argon (Fig. 4b) and on $LaAlO_3$ substrates under oxygen (Fig. 5a) and argon (Fig. 5b). In Fig. 4a, six well defined poles (marked by symbol *) are observed at a declination angle ψ equal to 35.3°, i.e. the value expected for In_2O_3 crystallites (1 1 1) oriented. Such poles lead to the following

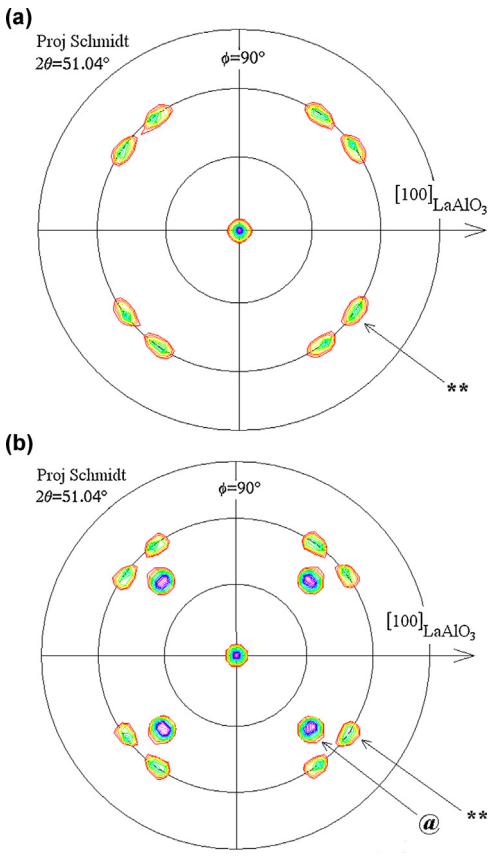

Fig. 5. Pole figures of the (0 4 4) In_2O_3 planes for films grown on $LaAlO_3$ substrates at 500 °C in O_2 (a) and Ar (b). The symbol ** is assigned in figure (a) and (b) to eight poles at every 60° of the In_2O_3 crystallites (0 1 1) oriented. In figure (b) four poles assigned with the @ symbol and located at every 45° correspond to In_2O_3 crystallites (0 0 1) oriented. The central pole corresponding to the (0 1 1) texture is present in figures (a) and (b).

in-plane epitaxial relationship between the film an c-cut sapphire substrate:$[1\text{–}10]_{In_2O_3}//[0\text{–}110]_{Al_2O_3}$

Such an epitaxial relationship has been already reported [28], and correspond to a 30° rotation of the hexagons of the (1 1 1) In_2O_3 bixbyite plane with respect to the hexagons of the (0 0 0 1) sapphire substrate. This leads to a good matching of the hexagonally packed In plane of In_2O_3 (1 1 1) with the closed packed oxygen plane of sapphire c-cut, as previously noted [28,29]. This in-plane epitaxial relationships which means a large mismatch between film and substrate (more than 50%) according to the values of axis parameter (1.43 and 0.824 nm for In_2O_3 and Al_2O_3, respectively) can be explained in the frame of the domain matching epitaxy or extended atomic distance mismatch approach [29,30]. In this approach, "m" lattice units of the film match with "p" lattice units of the substrate, i.e. $md_f \approx pd_s$ or $(d_f/d_s) \approx (p/m)$, with d_f and d_s being the respective atomic distances in the film and substrate parallel directions. The corresponding lattice mismatch δ can thus be defined by [31]:$\delta = \frac{2[md_f - pd_s]}{[md_f + pd_s]}$

The corresponding matching relationships and lattice mismatch are given in Table 1, which shows that in this approach the mismatch is reduced to 0.8%.

For the film grown on c-cut sapphire under argon ambient, Fig. 4b shows twelve well defined poles (assigned with the # symbol), at $\Psi = 45°$, i.e. the value expected for the (0 4 4) poles of In_2O_3 crystallites grown with the (0 0 1) texture (see Fig. 2). The following in-plane epitaxial relationships are deduced:$[1\text{–}10]_{In_2O_3}//[1\text{–}210]_{Al_2O_3}$ and $[1\text{–}10]_{In_2O_3}//[0\text{–}110]_{Al_2O_3}$

In addition, six other poles (assigned with the * symbol), are observed in Fig. 4b, located at $\Psi = 35.3°$, corresponding to In_2O_3 crystallites with the (1 1 1) texture. The in-plane epitaxial relationship which can be deduced is the following:$[1\text{–}10]_{In_2O_3}//[1\text{–}210]_{Al_2O_3}$

This relation is different from that observed in the film grown under oxygen. Indeed, in the present case this relation corresponds to a "hexagon" on "hexagon" growth for the (1 1 1) In_2O_3 plane on the (0 0 0 1) substrate. Such a situation is not the most likely in terms of interfacial energy. Indeed, in this configuration as noted previously the In ions from the films and O ions of the substrate do not coincide optimally [28,29]. The matching relationship and lattice mismatch given in Table 1 are therefore different from the case of films grown under oxygen. Moreover, Fig. 4b also shows that three of these six poles due to (1 1 1) crystallites are much intense than the others.

Such a situation has been already observed for In_2O_3 films grown under oxygen at a lower temperature [8]. The interpretation which has been proposed is based on the existence of two kinds of (1 1 1) In_2O_3 oriented crystallites in the films, i.e. crystallites with different in-plane symmetry: three-fold and six-fold symmetry. In the bixbyite structure, 25% of the oxygen sites are not occupied. This gives a specific arrangement of "constitutional" oxygen vacancies network, along the body diagonal and face diagonal of the cubic cell [32], which leads to a three-fold symmetry in the (1 1 1) plane. However, if some disorder is introduced in the network of "constitutional" oxygen vacancies (random distribution of the vacancies in the plane), the three-fold symmetry is no longer preserved, and a six-fold symmetry will appear in the (1 1 1) plane as it is the case in the fluorite structure [32].

In Fig. 5a, corresponding to film grown under oxygen on $LaAlO_3$, in addition to the central pole corresponding to the (0 1 1) texture deduced from the X-ray diffraction diagrams (Fig. 4), eight poles (assigned with the ** symbol), are present at $\Psi = 60°$ for the film grown on $LaAlO_3$. These poles correspond to In_2O_3 crystallites (0 1 1) oriented presenting the following in-plane epitaxial relationships:$[100]_{In_2O_3}//[100]_{LaAlO_3}$ and $[1\text{–}10]_{In_2O_3}//[010]_{LaAlO_3}$

Table 1 summarizes the results of the domain matching epitaxy approach for these relationships and shows that for the two orientations the lattice mismatch is limited (lower than 1%).

For the film grown under argon on $LaAlO_3$ substrate (Fig. 5b), in addition to the eight poles at $\Psi = 60°$ corresponding to In_2O_3 crystallites with the (0 1 1) texture (already observed in Fig. 5a), four poles located at $\Psi = 45°$ are also present (assigned with the @ symbol). This declination angle is expected for In_2O_3 crystallites (0 0 1) oriented. The in-plane epitaxial relationship which is deduced is the following:

$[1\text{–}10]_{In_2O_3}//[010]_{LaAlO_3}$

The matching relationships and lattice mismatch are summarized in Table 1, which shows low value of lattice mismatch (<1%) for all the epitaxial relationships.

The physical properties of these In oxide films were studied and Fig. 6 compares the absorption coefficient (α) in the form $(\alpha h\nu)^2$ versus photon energy ($h\nu$) [14,24] for films grown on c-cut substrates at 500 °C in oxygen and argon, respectively. The inset shows corresponding transmittance spectra in the 300–900 nm range. The films grown in oxygen are fully transparent (average transmittance of 90% at 500 nm) to the visible light while those grown in argon are less transparent (about 50% at 500 nm). In Fig. 6, the extrapolation of the linear portion of absorption plot gives an estimate of the optical band gap (E_g) of the In_2O_3 films and yields ~3.67 eV for oxygen and 3.69 eV for argon, which agrees well with the 3.75 eV value for the bulk value of In_2O_3 and films [14,24]. These values and those of the resistivity, density and mobility of the carriers deduced from Hall measurements are given in Table 2 for the films grown on c-cut sapphire and $LaAlO_3$ substrates.

Table 1

Gas ambient	Substrate	Texture	In-plane orientation	Matching relationships	Lattice mismatch
Oxygen	Sapphire	(1 1 1)	$[1\text{–}10]_{In_2O_3}//[0\text{–}110]_{Al_2O_3}$	$4d_f \approx 7d_s$	$\delta = 0.83\%$
Oxygen	$LaAlO_3$	(0 1 1)	$[100]_{In_2O_3}//[100]_{LaAlO_3}$	$3d_f \approx 8d_s$	$\delta = 0.138\%$
			$[1\text{–}10]_{In_2O_3}//[010]_{LaAlO_3}$	$4d_f \approx 15d_s$	$\delta = 0.64\%$
Argon	Sapphire	(0 0 1)	$[1\text{–}10]_{In_2O_3}//[1\text{–}210]_{Al_2O_3}$	$d_f \approx 3d_s$	$\delta = 0.165\%$
			$[1\text{–}10]_{In_2O_3}//[0\text{–}110]_{Al_2O_3}$	$4d_f \approx 7d_s$	$\delta = 0.83\%$
		(1 1 1)	$[1\text{–}10]_{In_2O_3}//[1\text{–}210]_{Al_2O_3}$	$d_f \approx 3d_s$	$\delta = 0.165\%$
Argon	$LaAlO_3$	(0 0 1)	$[1\text{–}10]_{In_2O_3}//[010]_{AlO_3}$	$4d_f \approx 15d_s$	$\delta = 0.64\%$
		(0 1 1)	$[100]_{In_2O_3}//[100]_{LaAlO_3}$	$3d_f \approx 8d_s$	$\delta = 0.138\%$
			$[1\text{–}10]_{In_2O_3}//[010]_{AlO_3}$	$4d_f \approx 15d_s$	$\delta = 0.64\%$

Table 2

Substrate		Resistivity (Ω cm)	Mobility ($cm^2/V\,s$)	Carrier density (cm^{-3})	Band gap (eV)
Sapphire c-cut*	Oxygen	2.67×10^{-1}	5.43	4.31×10^{18}	3.67
	Argon	5.35×10^{-4}	14.51	8.04×10^{21}	3.69
$LaAlO_3$**	Oxygen	2.74×10^{-1}	5.57	4.10×10^{18}	–
	Argon	4.67×10^{-4}	16.11	8.30×10^{20}	–

*Double side epipolished.
**One side epipolished.

It must be noticed, that the films grown in the same conditions on sapphire and $LaAlO_3$ single crystal substrates give similar results, i.e. only slight differences (a few %) in resistivity, carrier density and mobility were observed according to the substrate nature. This means that differences in texture and epitaxial relationships do not have a noticeable influence on the transport properties of In oxide films [7,13,33]. On the contrary, the oxygen composition of the films plays a major role on the physical properties (see Table 2). Actually, the oxygen vacancies concentration appears as the pertinent parameter controlling the transport properties in such films [7,34].

4. Discussion

The surface morphology of the indium oxide depends upon the growth conditions. The surface of films grown in argon gas present nanostructures whose density and size increase with temperature. The temperature which induces crystallization of the nanoparticles plays a role on the nanostructure formation, but it has been also observed that the films grown at the same temperature in oxygen gas do not present the same surface nanostructures. The temperature is not the sole parameter, and the precise nature of the indium oxide film as a function of the ambient gas during the growth has to be taken into account. Indeed, we have observed in this work, in agreement with previous reports [15,21,22] that the PED growth in argon [15] leads to the formation of In clusters through the phase separation of sub-stoichiometric In oxide [21,22]. Such In clusters could play a role on the formation of the observed surface nanostructures, in a way similar to that recently reported for Ga oxide films [23]. Actually, it has been reported that Ga clusters play the role of seeds to the growth of nanostructures (nanowires) by self-catalytic vapor–liquid–solid process (VSL) during Ga oxide films growth [23]. By comparison, in our work the In clusters which are formed by phase separation during the growth, could play the role of In seeds for a self catalytic VSL process leading to the growth of In oxide nanostructures. Further investigations are of course required in order to check this assumption.

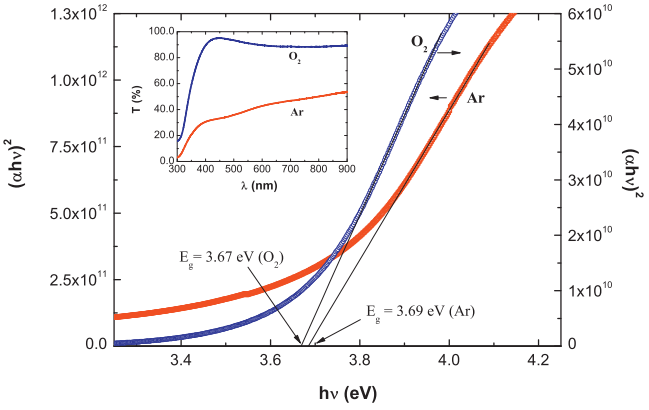

Fig. 6. $(\alpha h\upsilon)^2$ vs. $h\upsilon$ for In_2O_3 films grown on c-cut sapphire substrates at 500 °C at 2×10^{-2} mbar O_2 (a) and in Ar (b). The inset shows the corresponding optical transmittance of films.

Depending upon the substrate and ambient gas during PED, various film textures are observed in this work. Following surface free energy considerations for the In_2O_3 bixbyite phase, the (1 1 1) texture should be preferentially observed since the high atomic density (1 1 1) plane of the bixbyite present a lower surface free energy than the (0 1 1) and polar (0 0 1) planes, as it has been previously discussed [35,36]. However, (0 0 1) oriented In_2O_3 films can be grown under In-rich conditions [37], due to the incident indium species reaching the substrate surface. Such In species will play a key role by acting as an auto surfactant that lowers the surface free energy difference between the (0 0 1) and (1 1 1) surface [37]. During PED, the In species reaching the surface of the substrate directly come from the target, while the oxygen species come from both the target and oxygen pressure in the chamber. This means that the ratio of the In to O species fluxes on the substrate will depend upon the nature of the gas during PED. Comparing the growth conditions in oxygen and argon, it comes that the first case leads to oxygen-rich conditions favouring the (1 1 1) textured In_2O_3 growth. The absence of the (0 1 1) texture for the growth on c-cut sapphire substrate should be related to the difference in symmetry between the (0 0 0 1) sapphire plane and the two-fold symmetry of the (0 1 1) In_2O_3 plane, leading to higher interfacial energy for the (0 1 1) texture. On the other hand, PED under argon will lead to

In-rich conditions favouring the (0 0 1) textured In_2O_3 growth. The results observed on c-cut sapphire substrate are thus mainly related to these surface free energy considerations with a pure (1 1 1) In_2O_3 growth under oxygen, and both (1 1 1) and (0 0 1) textured In_2O_3 growth under argon. In that case, the (1 1 1) oriented crystallites present a "hexagon on hexagon like" epitaxial relationships with the substrate which is not the most favourable orientation [28,29]. The growth conditions with a high ratio of the In to O fluxes favours thus this orientation, but the reason why is not yet explained.

In the case of $LaAlO_3$ substrates, in addition to surface free energy consideration, the epitaxial growth of the In_2O_3 films has to be taken into consideration. Indeed, as previously reported [35,36] the difference between the free energy of the (1 1 1) and (0 1 1) In_2O_3 surfaces is rather small. As a result, the interfacial energy related to the epitaxial growth will be a pertinent parameter. In this frame, the respective symmetry of the (1 1 1) (three fold) and (0 1 1) (two fold) In_2O_3 planes are such that the epitaxial growth of the (0 1 1) plane on the cubic $LaAlO_3$ substrate will be favoured during the growth under oxygen. Actually, the small (1 1 1) textured growth observed in the diffraction diagram corresponds to polycrystalline In_2O_3, while epitaxial (0 1 1) growth is obtained. For the growth under argon, as seen above, the surface free energy of the (0 0 1) In_2O_3 plane will be reduced and as a result (0 0 1) and (0 1 1) textured growth are observed in these conditions.

Despite the differences in the structural characteristics (texture and epitaxial relationships) of the indium oxide films grown on c-cut sapphire and $LaAlO_3$ single crystal substrates, the physical properties of these films do not present large differences. Indeed, a variation of only few % in carrier mobility was observed, meaning that measurable effect of the crystalline structure of indium oxide on the carrier mobility is not evidenced. The origin of such behaviour is still a matter of discussion. On the contrary, the oxygen composition of the indium oxide films plays a major role on their optical and transport properties. Indeed a drastic increase in both carrier density and mobility is observed for the films grown under Ar, i.e. the films with a high oxygen deficiency. This change can be due to both an increase of the concentration of oxygen vacancy, acting as donor-doping and to the presence of metallic In clusters in such oxygen deficient In oxide films as deduced from the XRD patterns.

5. Conclusion

Indium oxide thin films were grown by pulsed electron beam deposition method on c-cut sapphire and $LaAlO_3$ single crystalline substrates under oxygen or argon pressure, respectively. Stoichiometric In_2O_3 films are grown under oxygen, while largely oxygen deficient In oxide films are formed under argon, i.e. in fact nanocomposite films with In metallic nanoclusters embedded in a In_2O_3 matrix are observed in this last case. Whatever the gas ambient during the growth epitaxial films with various orientation relationships and physical properties are obtained. The precise texture and epitaxial relationships are correlated to the growth conditions, while the oxygen composition determines the physical properties.

Acknowledgements

M. Nistor would thank a grant of the Romanian National Authority for Scientific Research, CNCS–UEFISCDI, project number PN-II-ID-PCE-2011-3-0566. The cooperative structure around SAFIR (Université Pierre et Marie Curie-Paris 6) is acknowledged for the RBS measurements.

References

[1] C.G. Granqvist, Appl. Phys. A 57 (1993) 19–24.
[2] C.Y. Wang, M. Ali, T. Kups, C.C. Rohlig, V. Cimalla, T. Standen, O. Ambacher, Sensors Actuators B 130 (2008) 589–593.
[3] Y. Zhang, H. Ago, J. Liu, M. Yumura, K. Uchida, S. Oshima, S. Ijima, J. Zhu, X. Zhang, J. Cryst. Growth 264 (2004) 363–368.
[4] J. Lao, J. Huang, D. Wang, Z. Ren, Adv. Mater. 16 (2004) 65–69.
[5] P.D.C. King, T.D. Veal, F. Fuchs, C.Y. Yang, D.J. Payne, A. Bourlange, H. Zhang, G.R. Bell, V. Cimalla, O. Ambacher, R.G. Egdell, F. Bechstedt, C.F. McConville, Phys. Rev. B 79 (2009) 205211–205310.
[6] H. Nakazawa, Y. Ito, E. Matsumoto, K. Adachi, N. Aoki, Y. Ochiai, J. Appl. Phys. 100 (2006) 93706–93708.
[7] A. Lany, T.O. Zakutayev, J.F. Mason, K.R. Wager, J.D. Poppelmeier, J.J. Perkins, D.S. Berry, A. Ginley, Zunger, Phys. Rev. Lett. 108 (2012) 16802–16805.
[8] W. Seiler, M. Nistor, C. Hebert, J. Perrière, Solar Energy Mater. Solar Cells 116 (2013) 34–42.
[9] Ch.Y. Wang, L. Kirste, F.M. Morales, J.M. Manuel, C.C. Röhlig, K. Köhler, V. Cimalla, R. Garcia, O. Ambacher, J. Appl. Phys. 110 (2011) 93712–93717.
[10] F. Yang, J. Ma, X. Feng, L. Kong, J. Cryst. Growth 310 (2008) 4054–4057.
[11] K.H.L. Zhang, D.J. Payne, R.G. Palgrave, V.K. Lazarov, W. Chen, A.T.S. Wee, C.F. McConville, P.D.C. King, T.D. Veal, G. Panaccione, P. Lacovig, R.G. Egdell, Chem. Mater. 21 (2009) 4353–4355.
[12] O. Bierwagen, J.S. Speck, Appl. Phys. Lett. 97 (2010) 72103–72113.
[13] T. Koida, M. Kondo, J. Appl. Phys. 99 (2006) 123703–123706.
[14] A. Dixit, C. Sudakar, R. Naik, V.M. Naik, G. Lawes, Appl. Phys. Lett. 95 (2009) 192105–192113.
[15] M. Nistor, J. Perrière, C. Hebert, W. Seiler, J. Phys. Condens. Matter 22 (2010) 45006–45007.
[16] S. Degoy, J. Jimenez, P. Martin, O. Martinez, A.C. Prieto, D. Chambonnet, C. Audry, C. Belouet, J. Perriere, Physica C 256 (1996) 291–297.
[17] L.R. Doolittle, Nucl. Instr. Methods B 9 (344) (1985) 344–351.
[18] E. Le Boulbar, E. Millon, J. Mathias, C. Boulmer-Leborgne, M. Nistor, F. Gherendi, N. Sbaï, J.B. Quoirin, Appl. Surf. Sci. 257 (2011) 5380–5383.
[19] R. Perez-Casero, J. Perrière, A. Gutierrez-Llorente, D. Defourneau, E. Millon, W. Seiler, L. Soriano, Phys. Rev. B 75 (2007) 165317–165327.
[20] S. Lany, A. Zunger, Phys. Rev. Lett. 98 (2007) 45501–45504.
[21] E. Millon, M. Nistor, C. Hebert, Y. Davila, J. Perrière, J. Mater. Chem. 22 (2012) 12179.
[22] J. Perrière, C. Hebert, A. Petitmangin, X. Portier, W. Seiler, M. Nistor, J. Appl. Phys. 109 (2011) 123704–123708.
[23] S.Y. Park, S.Y. Lee, S.H. Seo, D.Y. Noh, H.C. Kang, Appl. Phys. Express 6 (2013) 105001.
[24] C.Y. Wang, V. Cimalla, H. Romanus, Th. Kups, G. Ecke, Th. Stauden, M. Ali, V. Lebedev, J. Pezoldt, O. Ambacher, Appl. Phys. Lett. 89 (2006) 11904–11913.
[25] L. Nagarajan, R.A. De Souza, D. Samuelis, I. Valov, A. Börger, J. Janek, K.D. Becker, P.C. Schmidt, M. Martin, Nature Mater. 7 (2008) 391–398.
[26] A. Petitmangin, B. Gallas, C. Hebert, J. Perrière, L. Binet, P. Barboux, X. Portier, Appl. Surf. Sci. 278 (2013) 153–157.
[27] D. Roditchev, P. Lavallard, E. Dooryhée, A. Slaoui, J. Perrière, M. Gandais, Y. Wang, Nucl. Instrum. Methods B 107 (259) (1996) 259–262.
[28] Z.X. Mei, Y. Wang, X.L. Du, Z.Q.H. Zheng, J.F. Lia, Q.K. Xue, Z. Zhang, J. Cryst. Growth 289 (2009) 686–689.
[29] K.H.L. Zhang, V.K. Lazarov, P.L. Galindo, F.E. Oropeza, D.J. Payne, H.H.C. Lai, R.G. Egdell, Cryst. Growth Des. 12 (1000) (2012) 1000–1007.
[30] J. Narayan, K. Dovidenko, A.K. Sharma, S. Oktyabarsky, J. Appl. Phys. 84 (1998) 2597–2601.
[31] P.R. Willmott, R. Timm, J.R. Huber, Appl. Surf. Sci. 127–129 (1998) 105–110.
[32] B. Lacroix, F. Paumier, R.J. Gaboriaud, Phys. Rev. B 84 (2011) 14104–14112.
[33] A. Walsh, J.L.F. Da Silva, S.H. Wei, C. Korber, A. Klein, L.F.J. Piper, A. De Masi, K.E. Smith, G. Panaccione, P. Torelli, D.J. Payne, A. Bourlange, R.G. Egdell, Phys. Rev. Lett. 100 (2008) 167402–167404.
[34] M. Himmerlich, Ch.Y. Wang, V. Cimalla, O. Ambacher, S. Krischok, J. Appl. Phys. 111 (2012) 93704–93706.
[35] K.H.L. Zhang, A. Walsh, C.R.A. Catlow, V.K. Lazarov, R.G. Egdell, Nano Lett. 10 (2010) 3740–3746.
[36] A. Bourlange, D.J. Payne, R.G. Palgrave, J.S. Foord, R.G. Egdell, R.M.J. Jacobs, A. Schertel, J.L. Hutchinson, P.J. Dobson, Thin Solid Films 517 (2009) 4286–4294.
[37] O. Bierwagen, M.E. White, M.-Y. Tsai, J.S. Speck, Appl. Phys. Lett. 95 (2009) 262105–262113.